Proceedings of the ASME 2021
Fluids Engineering Division Summer Meeting
FEDSM2021
August 10-12, 2021, Virtual, Online

FEDSM2021-60958

PARAMETRIC STUDY ON WING-LAMBDA-SHOCK FORMATION

Sirikorn Chainok **Thanapol Rungroch** **Pattarasuda Chairach**

Prasert Prapamonthon* **Soemsak Yooyen**

Key Laboratory for Computational Mechanics & Heat Transfer Applications,
Department of Aeronautical Engineering, International Academy of Aviation Industry,
King Mongkut's Institute of Technology Ladkrabang, Bangkok 10520, Thailand

Bo Yin **Guowei Yang** **Shengjun Ju**
Key Laboratory for Mechanics in Fluid Solid Coupling Systems,
Institute of Mechanics, Chinese Academy of Sciences, Beijing, 100190, China

ABSTRACT

It is well-known that a wing is one of the most important parts of an aircraft as it is used to generate lift force. According to a wing moving at sufficiently high subsonic speeds, the flow speed on the wing's upper surface can be supersonic due to acceleration through the curvature-created suction, thereby forming a shock wave in a lambda shape. Additionally, the lambda shock can interact with the boundary layer flow. These phenomena relate to disturbances in the flow field, including flow separation, thus causing undesirable effects on lift production. Hence, a better understanding of the phenomenon of wing-lambda-shock formation and its nature is essential. This study presents a numerical investigation of the lambda-shock formation on an ONERA M6 wing, which is known as a swept, semi-span wing with no twist, under parametric effects of angle-of-attack, and free-stream Mach number, which is increased up to the supersonic regime. The pressure coefficients obtained by simulations are validated by open data. Then, numerical results in terms of the local pressure coefficient, local Mach number, averaged lift and drag coefficients, and λ-shape characteristics based on Mach number and pressure coefficients are discussed under an investigated range of the parameters. Results show that the angle-of-attack and free-stream Mach number can affect the lambda shock formation on the wing upper surface physically. Specifically, an iso-sonic surface with lambda shock waves is disturbed when the angle-of-attack and free-stream Mach number vary in an investigated range. This also affects lift and drag coefficients of the wing.

Keywords: Shock, transonic flow, supersonic flow

NOMENCLATURE

a	normalized root chord
A	wing area (m^2)
AOA	angle of attack (degree)
c	normalized mean-aerodynamic chord
C_d	drag coefficient
C_l	lift coefficient
C_p	pressure coefficient
F_d	drag force (N)
F_l	lift force (N)
L	normalized semi-span
Ma	Mach number
Ma_∞	freestream Mach number
P_d	dynamic pressure (Pa)
P_s	static pressure (Pa)
P_∞	freestream pressure (Pa)
Re	Reynolds number
s	arbitrary distance along wing-span direction
T_∞	freestream temperature (K)
U	air velocity (m/s)
v	local velocity (m/s)
v_s	sound speed (m/s)
ρ	air density (kg/m^3)

1. INTRODUCTION

It is well-known that Mach number (Ma) is used to classify flow regimes i.e. incompressible, subsonic, sonic, supersonic, and hypersonic. A flow regime that consists of high subsonic and low supersonic local flows in the same flow field is usually

* Corresponding author: prasert.pr@kmitl.ac.th

termed transonic and the freestream Mach number (Ma_∞) is typically in a range from 0.6 or 0.7 to 1.2. Under the circumstances of the transonic flow, a shock wave plays a major role in the local flow field. Namely, the supersonic regime is ceased by the shock wave, thereby slowing down the flow speed to the subsonic regime. This accounts for the λ-shock formation. Certainly, this phenomenon is also found on an aircraft wing moving in the subsonic regime. In fact, a wing is one of the most important parts of an aircraft as it is used to generate lift force. During a flight with sufficiently high subsonic speeds, the flow speed on the wing's upper surface can be supersonic due to acceleration through the curvature-created suction, thereby forming a shock wave in a λ-shape. Further complicated phenomena are also observed by the presence of the transonic flow such as the interaction between λ-shock and the boundary layer flow [1-3]. These phenomena relate to flow separation, thus causing a negative effect on lift production of the wing [4-5]. The ONERA M6 wing, which was experimentally reported by Schmitt and Charpin [6], is a typical example of a transonic wing that can perform the mentioned phenomena, as presented by Dwight [7]. Another observation of the transonic-flow phenomena on the ONERA M6 wing is discussed by Kuzmin [8]. His results indicated that the swept leading edge and the small curvature of an airfoil arc produce the formation of a λ-configuration of the local supersonic regions, thereby forming the λ-shape of pressure contours on the upper surface of the wing. Furthermore, the ONERA M6 wing has been widely used to validate computational results obtained by computation fluid dynamics, including further studies on the complicated phenomena of the transonic flow field and others [9-11]. So far, investigations on transonic flow also revealed the presence of a double supersonic-flow regime, including a formation of these regimes on airfoils that are comprised of a nearly flat arc [12-13]. Several studies indicated that the phenomena of the transonic flow can cause a pressure redistribution and a lift coefficient (C_l) jump on the upper surface of symmetric and asymmetric airfoils when two supersonic regions coalesce [14-15].

Although studies on the shock wave and flow separation, including demonstration of the λ-shape of isobars on the upper surface of transonic wings have been conducted experimentally and numerically for several years, it is still challenging because problems obtained by the phenomena of the shock wave and flow separation are complicated. In addition, the demonstration of the λ-shock formation can indicate the characteristics of flow physics happening to an airfoil. Hence, a better understanding of the nature of the λ-shape of isobars and others such as iso-Mach lines on the wing should be pointed out. Moreover, a further study on these phenomena in the supersonic region is also interesting. Therefore, the objectives of the present work are to numerically study the nature of the lambda-shock formation on the upper surface of a swept-back wing under effects of angle-of-attack (AOA), and freestream Mach number (Ma_∞), which increases to the supersonic regime. In fact, AOA and Ma_∞ are important parameters that can be controllable. A variation in these parameters can affect wing aerodynamic performance, and aircraft stability during a flight since AOA and Ma_∞ involve wing aerodynamic and aerothermal characteristics, respectively. Results obtained by the present study can provide significant information of lift and drag forces that are likely to relate to the presence of the wing-lambda-shock formation of a transonic wing.

2. WING MODEL, COMPUTATIONAL APPROACH, AND PARAMETERS

For this section, at first, a wing model with its geometry is introduced in subsection 2.1. Then, details of the computational approach computational meshes, numerical setups, and numerical validations are given in subsection 2.2. Lastly, aerodynamic parameters are specified in subsection 2.3.

2.1 Wing Model and Geometry

A wing model used in the present work is an ONERA M6 wing that is adopted from Schmitt and Charpin [6]. This wing is a semi-swept-back wing with no twist, as shown in Fig. 1(a). The wing geometry is normalized so that the semi-span, root chord, and mean aerodynamic chord are equal to 1, 0.6738, and 0.540, respectively, as shown in Fig. 1(b). Additionally, some important geometric details of the wing are listed in Table 1.

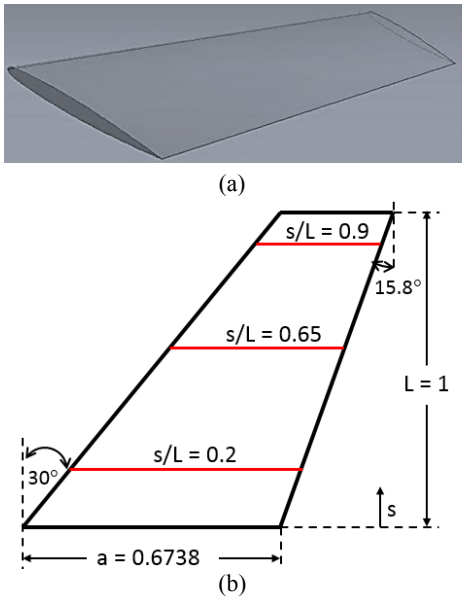

Figure 1: (a) Wing model in 3D, and (b) wing geometry.

Table 1: Geometric details of wing model

Characteristic figures	Value
Semi-span (L)	0.3048
Root chord (a)	0.6738
Mean-aerodynamic chord (c)	0.540
Aspect ratio	3.8
Taper ratio	0.562
Leading-edge sweep angle	30°
Trailing-edge sweep angle	15.8°

2.2 Computational Approach

The numerical simulation has been widely used in various industrial applications [16-22], and it is one of the main research approaches for aircraft aerodynamics due to the advantages of low cost and high efficiency. As mentioned previously, the numerical simulation is also used for the present work. Starting from a computational flow domain for the wing, the domain is created until it is large enough for obtaining acceptable results from boundary conditions, as shown in Fig. 2.

For properties of the fluid, the air is considered as a compressible gas. Therefore, the ideal gas law is used. Other thermodynamic properties are given as follows: 1) Specific heat capacity = 1.006 kJ/kg·K, 2) Thermal conductivity = 0.02420607 W/m·K, and 3) Dynamic viscosity = 1.62699 x 10^{-5} Pa·s.

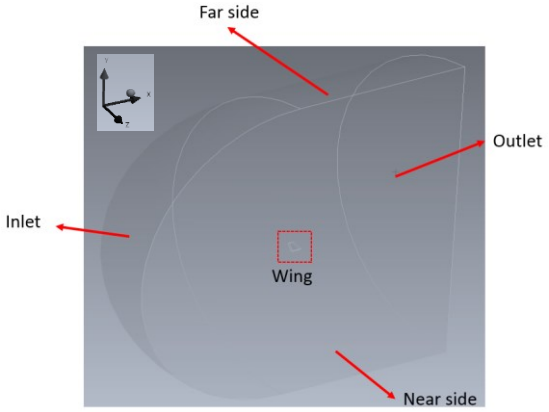

Figure 2: Computational flow domain for wing.

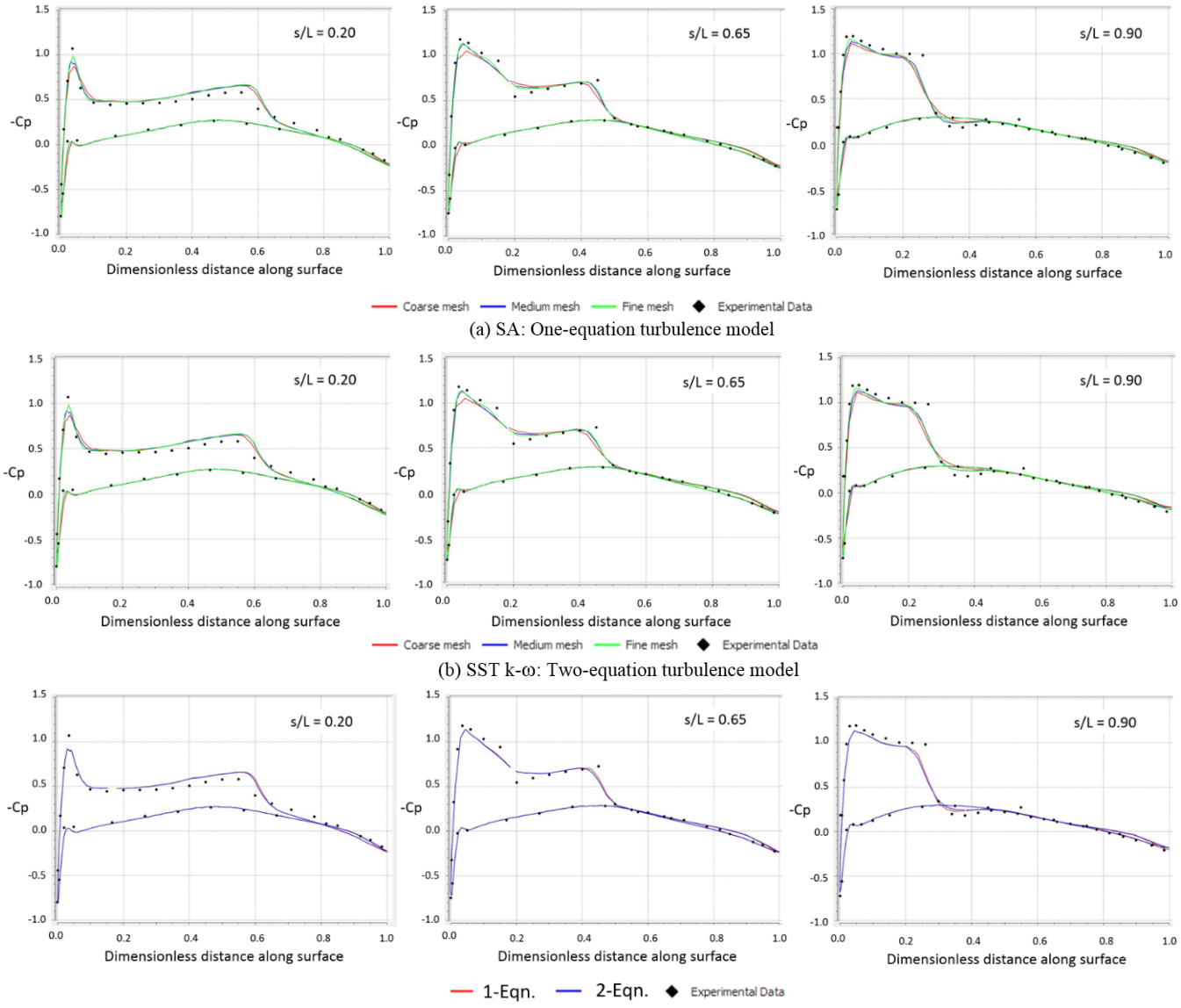

(a) SA: One-equation turbulence model

(b) SST k-ω: Two-equation turbulence model

(c) One-equation vs two-equation turbulence models for medium mesh

Figure 3: Mesh independence obtained by (a) SA: one-equation and (b) SST k- ω: two-equation turbulence models, and (c) comparison and validation of numerical results obtained from SA and SST k-ω turbulences for medium mesh.

For the initial setting of boundary conditions, according to Fig. 2, the pressure far field condition is given at the inlet, outlet, and far-side boundaries, whereas the symmetry condition is provided for the near-side boundary. Primary values of the boundary condition at the inlet, outlet, and far-side boundaries are set in accordance with an experiment conducted by Schmitt and Charpin [6], as follows: 1) $P_\infty = 0.316$ MPa, 2) $Ma_\infty = 0.8395$, 3) AOA = 3.06°, and 4) $T_\infty = 255.56$ K, thereby obtaining the Re $\approx 11.7 \times 10^6$ based on the normalized mean-aerodynamic chord. A set of results obtained by the primary values will be a benchmark for other solutions.

The computational mesh of the flow domain is a hybrid mesh of the structured and unstructured meshes that are generated by automatic mesh modeling. The structured mesh is formed in a quadrilateral element, whereas the unstructured mesh is made in a triangular shape. The structured mesh is used to provide the dense mesh with 10 layers in the region close to the wing surface. With this arrangement, phenomena of the lambda shock and boundary-layer flow can be observed. To confirm the mesh independence, a three-number mesh strategy is conducted by coarse, medium, and fine meshes, as given in Table 2.

Table 2: Mesh elements for mesh-independence strategy.

Mesh	Element numbers
Coarse	690,755
Medium	1,525,403
Fine	2,324,894

The ANSYS FLUENT is used as a solver for numerical solutions. The one-equation Spalart-Allmaras (SA) [23] and two-equation Shear Stress Transport (SST) k-ω [24] turbulence models with the second-order accuracy are employed. The mesh independence and validation of numerical results are done by comparing the distributions of the pressure coefficient defined by $C_p = \frac{P_s - P_\infty}{P_d}$ along the wing surface at three span positions i.e. s/L = 0.20, 0.65, and 0.90 corresponding to Fig. 1(b). As shown in Figs. 3(a) and 3(b), the results of C_p obtained by the medium and fine meshes at the three positions for both turbulence models have good agreements with acceptable errors. Besides, Fig. 3(c) shows the comparison and validation between the C_p results predicted by the two turbulence models for the medium mesh with open experimental data [6]. One can see that at the three positions, the distributions of C_p obtained by both turbulence models agree well with the experimental data. It should be noted that although the SA model can provide acceptable C_p values with low computational cost, it usually predicts less accurate solutions of flow separation and transition from smooth surfaces when compared to the SST k-ω turbulence model. Moreover, the investigated range of the aerodynamic parameters in the present study may involve strong transition and flow separation such as at AOA = 5°. Overall, the medium mesh and SST k-ω model are selected for the subsequent calculations.

Details of the medium mesh of the computational flow domain are presented in Fig. 4.

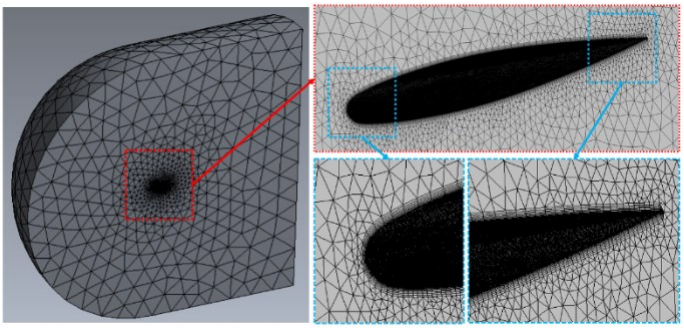

Figure 4: Medium mesh of computational flow domain and dense mesh close to wing surface.

2.3 Aerodynamic Parameters

As AOA and Ma_∞ are controllable factors that can produce positive and negative effects during a flight of an aircraft, an investigation into their effects on flow physics around wing surfaces is very important. To obtain a better understanding of a phenomenon of the lambda-shock formation on the wing surface under the effects of AOA and Ma_∞, the parametric study of AOA, and Ma_∞ is conducted. Investigated ranges of AOA and Ma_∞ are listed in Table 3.

Table 3: Values of aerodynamic parameters.

Parameters	Values*
AOA (degree)	0 - 5
Ma_∞	0.6 – 1.6

*Values of primary design for AOA, Ma_∞, and P_∞ are 3.06°, 0.8395, and 0.316 MPa, respectively.

In fact, the occurrence of the lambda shock affects the flow field, thereby resulting in drag and lift forces, which are usually used to evaluate wing performance. Therefore, the drag and lift forces are also evaluated by considering their coefficients that are defined as Eqs. (1) and (2), respectively.

$$C_d = \frac{2F_d}{\rho U^2 A} \quad (1)$$

and

$$C_l = \frac{2F_l}{\rho U^2 A} \quad (2)$$

It should be noted that C_d and C_l are average values. In addition, the local Ma number (Ma), which is defined as $Ma = \frac{v}{v_s}$, is presented to discuss shock-wave effects also.

3. RESULTS AND DISCUSSION

This section presents numerical results and discusses some phenomena observed from the results in terms of local Ma, C_p, C_d, and C_l so that the nature of the λ-shape is characterized. At

first, the benchmark case is given, Then, the effects of AOA, and Ma_∞ are presented.

3.1 Benchmark Case

To investigate characteristics of the wing-lambda-shock formation under effects of the aerodynamic parameters, a set of computational results obtained by the primary-design values is used for a benchmark. As illustrated in Fig. 5, at these values, a sonic surface is observed on the upper surface and iso-Mach lines of the supersonic regions occur at the cross-sectional areas, s/L = 0.65, and 0.90, whereas the transitional regions with slightly greater Mach numbers than 1 are located at the wing root (s/L = 0) and s/L = 0.20. One can see that at each cross-sectional area, a λ-shape of the shock wave is developed by the presence of the upstream supersonic shock near the leading edge (LE) and the downstream shock terminating the local supersonic regime on the upper surface. However, the size of the λ-shape decreases with the position in the spanwise direction (s/L). This also accounts for the λ formation of the sonic surface.

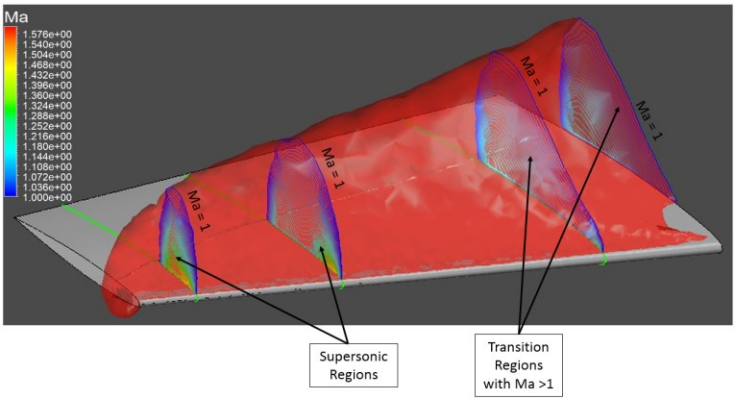

Figure 5: Sonic surface and iso-Mach lines along spanwise direction at s/L = 0, 0.20, 0.65, and 0.90 for benchmark case.

With a contour of C_p, a λ-configuration of C_p is displayed on the wing upper surface, as seen in Fig. 6. This phenomenon corresponds to the sonic surface previously shown in Fig. 5 and it indicates a major role of the swept LE and small arc LE of the wing. In addition, for this case, it yields C_d = 0.0094 and C_l = 0.1242.

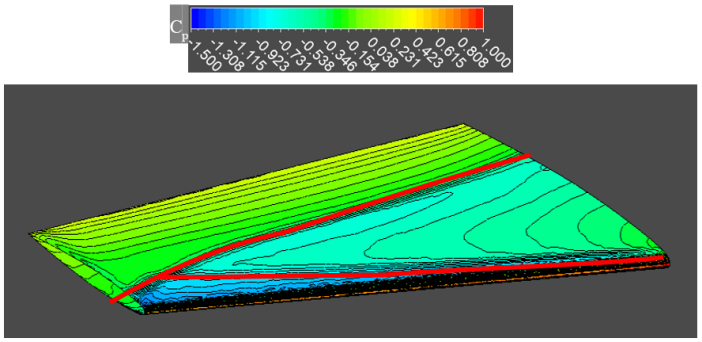

Figure 6: C_p distribution on wing upper surface for benchmark case.

3.2 Effects of AOA

To understand the influence of AOA on the nature of the λ-shock formation, an iso-surface of the sonic regime and iso-Mach lines at the three positions along the spanwise direction on the wing upper surface are presented, as shown in Fig. 7. Here, it should be noted that in this section, Ma_∞ keeps unchanged at the primary value of 0.8395 and AOA varies in the investigated range from 0° to 5°. It is seen that at AOA = 0°, small λ-shapes and a small sonic surface occur but the sonic surface cannot cover the wing upper surface near the LE in the range of s/L from 0 to 0.65. However, when AOA increases, the sonic surface expands and cover completely the upper surface near the LE at AOA = 5°. The expansion of the sonic surface corresponds to the iso-Mach lines, namely, the upstream leg of the λ-shapes moves forward to the LE. These phenomena may be because of a significant influence of the presence of the tip vortex and flow separation on the surface, as illustrated in Fig. 8.

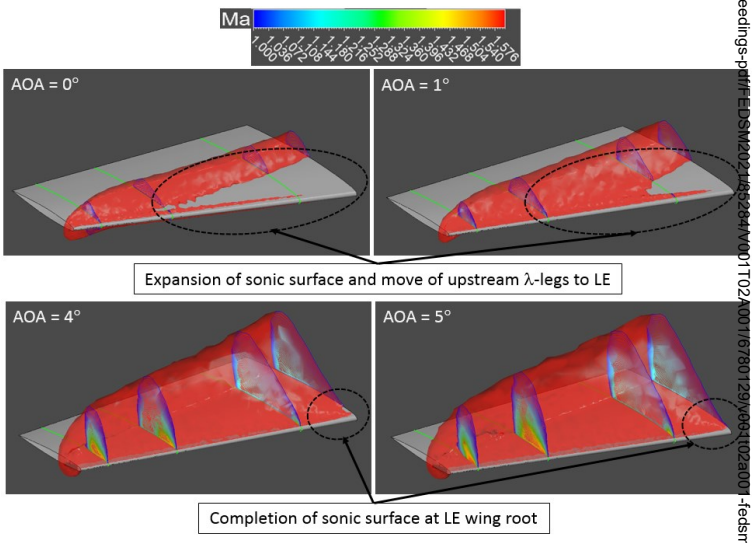

Figure 7: Effects of AOA on lambda shock formation based on local Mach numbers.

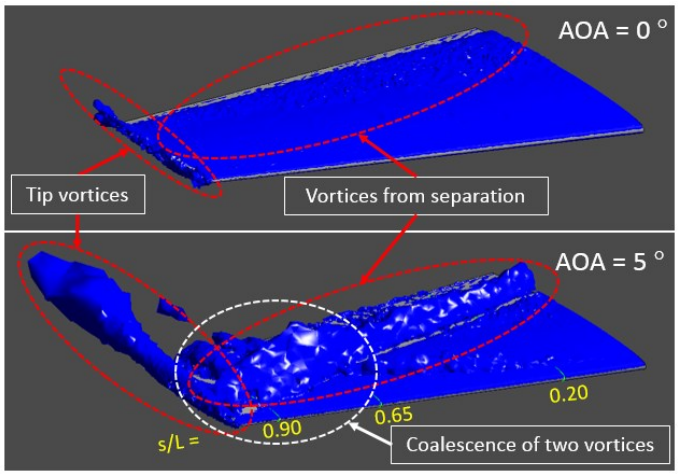

Figure 8: Influence of tip vortex at AOA = 0° and 5° with Q-criterion = 0.001.

Next, the distributions of C_p at s/L = 0.65 are discussed as at this position, the phenomenon of λ-shock formation appears obviously when AOA increases from 0° to 5°. As plotted in Fig. 9, the trends of the C_p distributions obtained at AOA = 0° - 2° are similar to one another. However, the trends of the C_p distributions change significantly when AOA increases to 3.06°, 4°, and 5°. This phenomenon indicates variations of the static and dynamic pressures affected by the coalescence of the tip vortex and vortices from flow separation, including the λ-shock waves performed by iso-Mach lines, as shown in a white circular frame in Figs. 8 and 10. The distributions of the C_p in the λ-shapes on the upper surface at AOA = 5° are also displayed in Fig. 11. The discrepancies between the λ-shock formation at AOA = 5° and the benchmark case, including other AOAs highlight the nature of the λ-shock formation based on C_p under the effects of AOA.

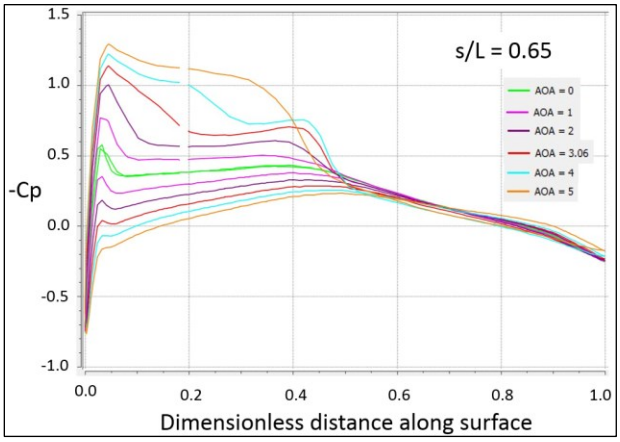

Figure 9: Effects of AOA on C_p at s/L = 0.65.

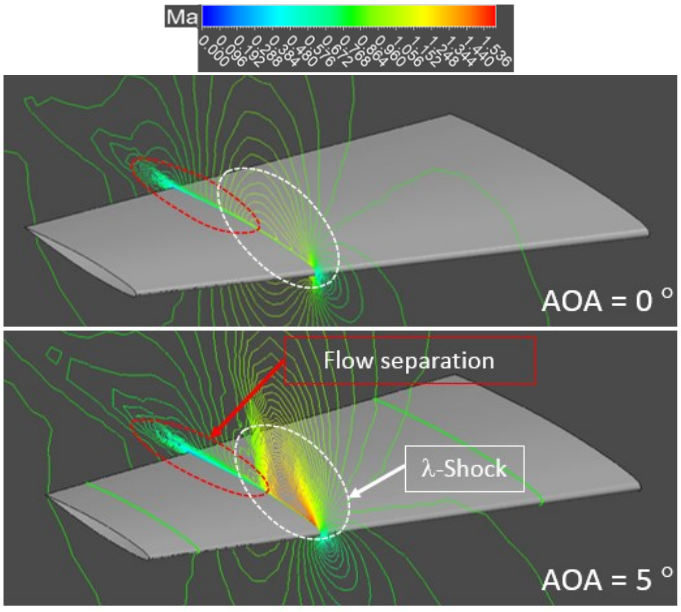

Figure 10: Iso-Mach lines and flow separation at at s/L = 0.65.

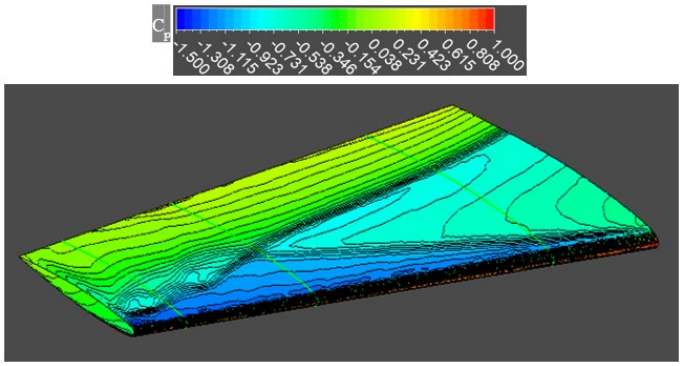

Figure 11: C_p distribution on wing upper surface at AOA = 5°.

Another observation is shown in Fig. 12. One can see that C_l increases linearly with AOA from AOA = 0° to 4°. However, C_l decreases at AOA = 5°. This indicates the occurrence of a stall phenomenon at this AOA. For C_d, C_d increases slightly when AOA changes from 0° to 4°, and C_d increases meaningfully at AOA = 5°, which relates to the decline in C_l. These variations of Cl and Cd correspond with the phenomena mentioned previously.

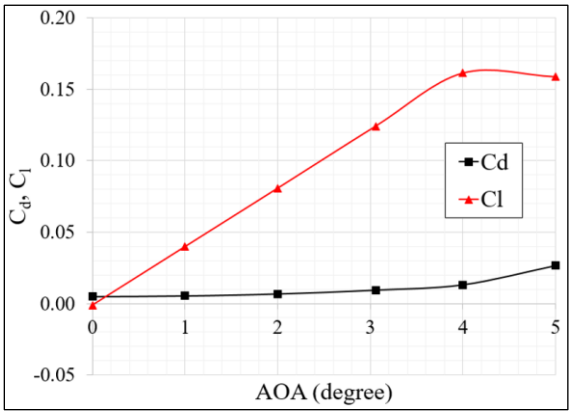

Figure 12: C_l and C_d at different AOAs.

3.3 Effects of Ma_∞

The effects of Ma_∞ on the nature of the λ-shock are discussed in this section. As expected, phenomena under the effects of Ma_∞ are likely to link variations of C_p, C_l, and C_d of the wing. In this section, the AOA keeps constant at 3.06° so that the Ma_∞ is a single independent parameter for the consideration.

As shown in Fig. 13, clearly, at a lower $Ma_\infty = 0.7$, the sonic surface with the λ-shock cannot be formed yet. When Ma_∞ increases to 0.8, it establishes the sonic surface with the strong λ-shock waves at s/L = 0.65 and 0.90. This is similar to the formation obtained by the benchmark case in Fig. 5. Then, at $Ma_\infty = 0.9$, the sonic surface with the λ-shock waves expands greatly and the surface largely covers all the upper surface. However, when Ma_∞ continues increasing to the sonic flow, two sonic surfaces exist at the LE and trailing edge (TE) instead. This seems that the initial sonic surface expands until it separates. As a result, the size of the λ-shock waves grows substantially.

Oppositely, at higher values of Ma_∞ in the supersonic regime, namely, at $Ma_\infty = 1.2$, the TE sonic surface disappears, whereas the LE sonic surface is in a reversal, specifically, the wing-surface detachment occurs. Consequently, the λ-shapes are not inside the sonic surface anymore. At $Ma_\infty = 1.4$, the extraction of the LE sonic surface is observed.

Likewise, the distributions of C_p at s/L = 0.65 are discussed as C_p varies with Ma_∞. Fig. 14(a) indicates that at the subsonic speeds, the trends of Cp are similar to one another except at Ma_∞ = 0.893, and 0.9. This may be explained by vortices developing on the upper surface, as seen in the yellow and white curves in Fig. 15(a). For the C_p distributions at the supersonic speeds, as presented in Fig. 14(b) obviously, the trends of the C_p distributions for all Ma_∞ are like the trend obtained at Ma = 1.0. Also, the phenomenon of the C_p distributions in the supersonic can be explained more by Fig. 15(b), in which significant differences of the vortices are found at the wing TE and wingtip.

To obtain a better understanding of the effects of Ma_∞, the C_p distributions on the surface at different values of Ma_∞ are presented in Fig. 16 as well. Interestingly, although the characteristics of the sonic surface at the sonic and supersonic speeds are different from those obtained by the subsonic speeds as earlier discussed, the λ-shapes based on C_p still exist. However, only a small size is observed at the LE-root wing at Ma_∞ = 1.6. This suggests that the λ-shape will disappear at adequately high supersonic speeds.

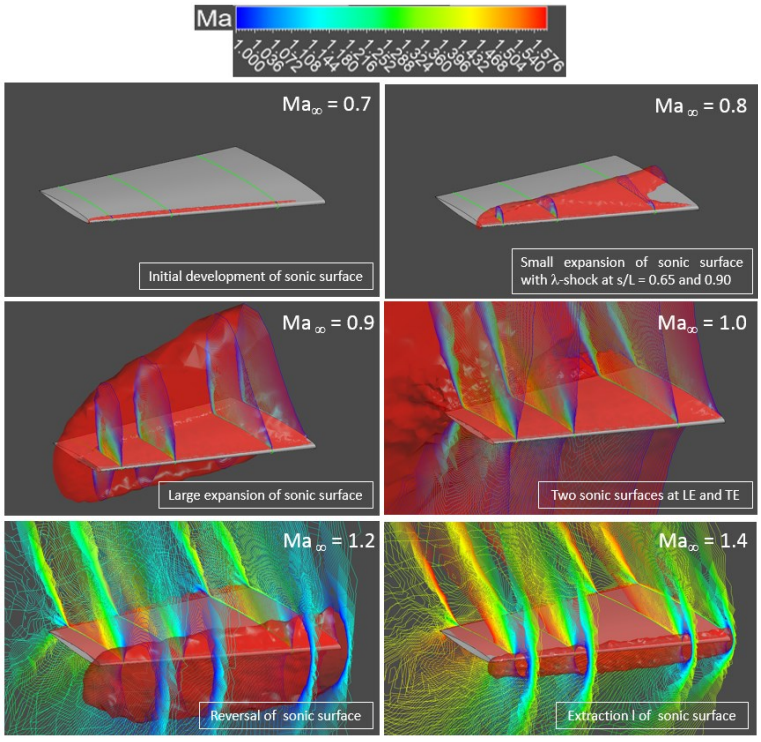

Figure 13: Effects of Ma_∞ on lambda shock formation based on local Mach numbers.

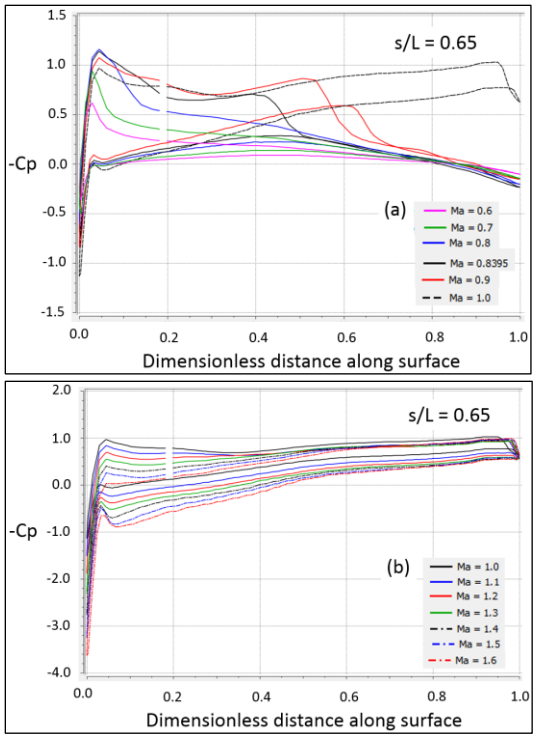

Figure 14: Effects of Ma_∞ on C_p at s/L = 0.65 when flow is (a) subsonic and (b) supersonic.

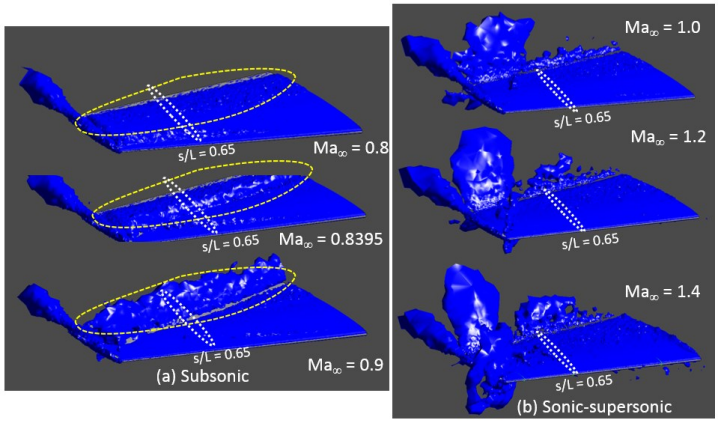

Figure 15: Vortices with Q-criterion = 0.001 on upper surface when (a) subsonic and (b) sonic-supersonic speeds of freestream are considered.

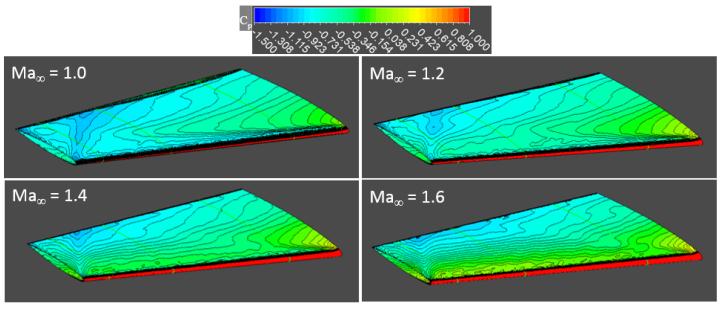

Figure 16: C_p distribution on wing upper surface when Ma_∞ increases from sonic to supersonic speeds.

Finally, C_l and C_d obtained by different Ma_∞ values are plotted in Fig. 17. At subsonic speeds Ma_∞ = 0.6 - 0.8395, C_d increases slightly, whereas C_l increases considerably until it reaches an approximate 136% increase at Ma_∞ = 0.8395. In addition, from Ma_∞ = 0.8395 onwards, significant increases in C_d are found. This seems similar to increments of C_l except at Ma_∞ = 0.95. Specifically, C_l drops at this Ma_∞ before surging at the sonic speed. This phenomenon may be explained by the fact that the flow field at Ma_∞ = 0.95 is affected by the presence of larger vortices on the lower surface when compared to vortices occurring at Ma_∞ = 0.90, as captured in Fig. 18. This leads to the drop of C_l and the significant increase of C_d at such Ma_∞.

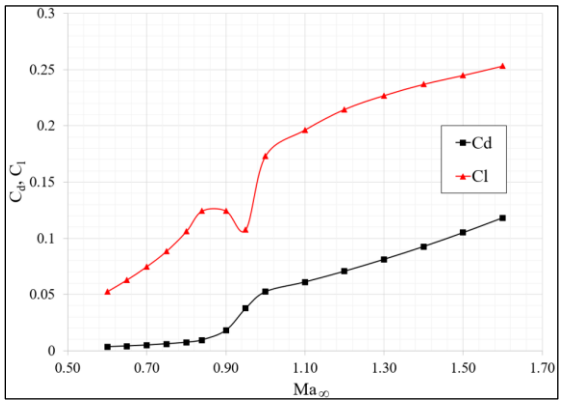

Figure 17: C_l and C_d at different values of Ma_∞.

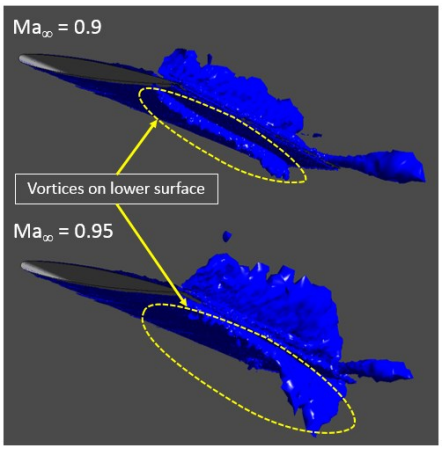

Figure 18: Comparison of vortices on lower surface at Ma_∞ = 0.9 and 0.95.

4. CONCLUSION

This study presents a numerical investigation of the lambda-shock formation on an ONERA M6 wing, which is known as a swept, semi-span wing with no twist, under parametric effects of angle-of-attack (AOA), and freestream Mach number (Ma_∞), which is increased up to the supersonic regime. The SST k-ω turbulence model is used to predict characteristics of the flow field and interesting phenomena. Numerical results in terms of the local pressure coefficient, local Mach number, averaged lift and drag coefficients, and λ-shape characteristics based on Mach number and pressure coefficients are discussed under an investigated range of the parameters i.e. AOA = 0° - 5° and Ma_∞ = 0.6 – 1.6. The numerical results show that an iso-sonic surface and iso-Mach lines are under the effects of AOA and this also affects the nature of the λ-shock formation based on Mach number. In addition, when the freestream Mach number is considered, the sonic surface with λ-shock waves expands with the freestream Mach number at subsonic speeds. This phenomenon corresponds to the λ-shape of C_p. However, a reversal with the detachment of the sonic surface is observed at supersonic speeds. Although at these high speeds, the sonic surface is not located on the upper surface, the λ-shape of C_p still exists on the upper surface and seems to vanish at sufficiently higher speeds. Also, these phenomena can affect C_l and C_d of the wing. The present work will fulfill the understanding of the phenomena of the lambda-shock formation and its collapse on other swept wings that are commonly caused by two key factors viz the swept leading edge and the small curvature of an airfoil suction arc.

ACKNOWLEDGEMENTS

This research is financially supported by the income funding provided by International Academy of Aviation Industry, King Mongkut's Institute of Technology Ladkrabang (Contract No: 2561-15-06) and the KMITL Research Fund of King Mongkut's Institute of Technology Ladkrabang under the program of Research Seed Grant for New Lecturer (Contract No. KREF186015).

REFERENCES

[1] Gatski, T.B., and Bonnet, J-P., 2013, "Chapter 8 - Elements of compressible flow control," Compressibility, turbulence and high speed flow," 2nd edition, Academic Press, Elsevier, pp. 271-292

[2] Délery, J.M., 2001, "Chapter 8.3 - Shock wave/boundary layer interactions," Handbook of shock waves, 2, Academic Press, Elsevier, pp. 205-264.

[3] Houghton, E.L., Carpenter, P.W., Collicott, S.H., and Valentine, D.T., 2017, "Chapter 3 - Viscous flow and boundary layers," Aerodynamics for engineering students, 7th edition, 2, Butterworth-Heinemann, Elsevier, pp. 151-254.

[4] Avelar, A.C., Filho, J.B.P.F., Leite, H.F., Annes da Silva, D.G., and Hsu, J., 2016, "Experimental study of shock wave patterns over an airfoil," 46th AIAA Fluid Dynamics Conference, Paper no. AIAA 2016-3935.

[5] Coschignano, A., Atkins, N., Babinsky, H., and Serna, J., 2019, "Effect of Reynolds number on a normal shock wave-transitional boundary-layer interaction over a curved surface," Exp. Fluids, 60, pp. 185.

[6] Schmitt, V., and Charpin, F., 1979, "Pressure distributions on the ONERA-M6-Wing at transonic Mach numbers," experimental data base for computer program assessment. report of the fluid dynamics panel working group 04, AGARD AR 138.

[7] Dwight, R.P., 2008, “Heuristic a posteriori estimation of error due to dissipation in finite volume schemes and application to mesh adaptation,” J. Comput. Physics, 227, pp. 2845–2863.
[8] Kuzmin, A., 2014, “On the lambda-shock formation on ONERA M6 wing,” Int. J. Appl. Eng. Res., 9(20), pp. 7029-7038
[9] Nambu, T., Hashimoto, A., Aoyama, T., and Sato, T.,2015, “Numerical analysis of the ONERA-M6 wing with wind tunnel wall interference,” T. Jpn. Soc. Aeronaut. S., 58(1), pp. 7-14.
[10] Mayeur, J., Dumont, A., Destarac, D., and Gleize, V., 2016, “Reynolds-averaged Navier–Stokes simulations on NACA0012 and ONERA-M6 wing with the ONERA elsA Solver,” AIAAJ, 54(9), pp. 1-17.
[11] Yamamoto, S., Hagari, H., and Murayama, M., 2000, “Numerical simulation of condensation around the 3-D wing, T. Jpn. Soc. Aeronaut. S., 42(138), pp. 182-18
[12] Jameson, A., 1991, “Airfoils admitting non-unique solutions of the Euler equations,” Paper no. AIAA 91-1625, pp. 1−14.
[13] Ivanova, A.V., and Kuzmin, A.G., 2004, “Nonuniqueness of the transonic flow past an airfoil,” Fluid Dyn., 39(4), pp. 642−648.
[14] Hafez, M., and Guo, W., 1999, “Some anomalies of numerical simulation of shock waves. Part II: Effect of artificial and real viscosity,” Comput. Fluids, 28, pp. 721–739.
[15] Kuzmin, A., 2013, “Transonic flow past a whitcomb airfoil with a deflected aileron,” Int. J. Aeronaut. Space Sci, 14(3), pp. 210−214.
[16] Luo, X.W., Huang, R.F., and Ji, B., 2016, “Transient cavitating vortical flows around a hydrofoil using k-omega partially averaged Navier-Stokes model,” Mod. Phys. Lett. B, 30(1), pp. 1550262.
[17] Luo, X.W., Ye, W.X, Huang, R.F., Wang, Y.W., Du, T.Z., and Huang, C.G., 2020, “Numerical investigations of the energy performance and pressure fluctuations for a waterjet pump in a non-uniform inflow,” Renew. Energy, 153, pp. 1042-1052.
[18] Zhao, X.L., and Sun Z.X., 2010, “A new method for numerical simulation of two trains passing by each other at the same speed,” J. Hydrodynam B, 22(5), pp. 697-702.
[19] Prapamonthon, P., Yin, B., Yang, G.W., 2019, “Extra-low Reynolds number vane separation using immersed boundary method,” Paper No. AJKFluids 2019-5077.
[20] Ju, S.J., Sun, Z.X., Yang, G.W., Prapamonthon, P., Zhang, J.Y., 2020, “Parametric study on drag reduction with the combination of the upstream energy deposition and the opposing jet configuration in supersonic flows,” Acta Astronaut., 171, pp. 300-310.
[21] Prapamonthon, P., Yooyen, S., and Sleesongsom, S., 2019, “CHT/CFD analysis of thermal sensitivity of a transonic gilm-cooled guide vane,” Comput. Model. Eng. Sci., 119(3), pp. 593-615.
[22] Prapamonthon, P., Yin, B., Yang, G.W., Zhang, M.H., 2020, “Separate and combined effects of surface roughness and thermal barrier coating on vane cooling performance,” J. Thermal. Sci. Eng. Appl., 12(5), pp. 051017.
[23] Spalart, P.R., and Allmaras, S.R., 1992, "A one-equation turbulence model for aerodynamic flows", AIAA Paper No. 92-0439.
[24] Menter, F.R., 2009, “Review of the shear-stress transport turbulence model experience from an industrial perspective,” Int. J. Comut. Fluid Dyn., 23(4), pp. 305−316.